Radiology Case Reports 20 (2025) 2513–2520

Available online at www.sciencedirect.com

ScienceDirect

journal homepage: www.elsevier.com/locate/radcr

Case Report

Two case reports of ovarian clear cell carcinoma: Atypical MRI findings with a renal corticomedullary contrast-like appearance ☆

Nobuyuki Takeyama[a,*], *Yasuo Ueda*[b], *Mutsuko Omatsu*[c], *Tetsuo Nemoto*[c], *Takashi Ogawa*[b], *Shingo Miyamoto*[d], *Kiyotake Ichizuka*[d], *Ken Nakayama*[e], *Miki Morioka*[e], *Hidefumi Fujisawa*[a]

[a] *Department of Radiology, Showa University Northern Yokohama Hospital, Yokohama-City, Tsuzuki-ku, Japan*
[b] *Department of Pathology and Laboratory Medicine, Showa University Fujigaoka Hospital, Yokohama-City, Kanagawa, Japan*
[c] *Department of Pathology and Laboratory Medicine, Showa University Northern Yokohama Hospital, Yokohama-City, Tsuzuki-ku, Japan*
[d] *Department of Obstetrics and Gynecology, Showa University Northern Yokohama Hospital. 35-1 Chigasakichuo, Tsuzuki-ku, Yokohama-City, 224-8503, Japan*
[e] *Department of Radiology, Showa University Fujigaoka Hospital, Yokohama-City, Kanagawa, Japan*

ARTICLE INFO

Article history:
Received 6 December 2024
Revised 23 January 2025
Accepted 25 January 2025

Keywords:
Clear cell carcinoma
Magnetic resonance imaging
Solid-type

ABSTRACT

The MR images of the two cases of ovarian clear cell carcinomas (CCCs), presenting as entirely solid-masses, revealed a band-like peripheral area and a geographic central area: The peripheral area images resembled those of the renal cortex, while the central area images resembled those of the renal medulla. Compared to the iliac muscle, the band-like peripheral area appeared iso-hyperintense on T2-weighted imaging (T2WI), isointense on unenhanced T1-weighted imaging (T1WI), hyperintense on diffusion-weighted imaging (DWI), and hypo-isointense on an apparent diffusion coefficient (ADC) map, with gradual enhancement on dynamic contrast-enhanced T1WI. The geographic central area of the tumor appeared hyperintense on T2WI, hypointense on T1WI, hypointense on DWI, and hyperintense on an ADC map, with less enhancement on dynamic contrast-enhanced T1WI. Simple total hysterectomy, salpingo-oophorectomy, and partial omentectomy were performed in both cases. Both tumors were entirely solid, and histopathological analysis revealed cancer cell proliferation accompanied by an increase in stromal fibrous tissue in the peripheral area. Edematous stroma and fibrosis were predominantly observed with minimal cancer cells in the central area. The patients were diagnosed with ovarian CCC (pT1a). The mechanism behind the appearance of peripheral and central areas with renal corticomedullary contrast in such

☆ Competing Interests: The authors declare that they have no known competing financial interests or personal relationships that could have appeared to influence the work reported in this paper.

* Corresponding author.
E-mail address: nobuyukitakeyama@gmail.com (N. Takeyama).

https://doi.org/10.1016/j.radcr.2025.01.091

cases remains unknown, and MRI can provide valuable insights for the differential diagnosis of epithelial ovarian cancer.

Introduction

Ovarian clear cell carcinoma (CCC) is a histological subtype of epithelial ovarian cancer with distinct clinical features. The cysts and glands are lined with cuboidal, hobnail, or flattened cells with a clear or eosinophilic cytoplasm [1]. CCC generally constitutes approximately 10% of epithelial ovarian cancer (OC) cases in Western countries [2] but accounts for 20%-25% of cases in Japan, although the reasons for these geographic differences in prevalence remain unclear [3]. While most patients are diagnosed at an early stage, advanced-stage CCC has a worse prognosis than serous or endometrioid carcinomas due to its relative insensitivity to platinum-based chemotherapeutic agents and is classified as a high-grade malignancy [4,5]. Gynecologists can make maximal efforts to achieve zero residual disease when CCC is identified preoperatively [6]. Therefore, it may be useful to estimate CCC preoperatively when interpreting magnetic resonance imaging (MRI). MRI findings of CCC have been reported in several studies [7,8]. CCC or endometrioid carcinoma is considered as endometriosis-associated OC when an ovarian cyst containing chocolate-colored fluid has a vascularized mural nodule in the wall, as observed on ultrasound [9–12]. CCC developing from endometriosis is more commonly visualized as a unilocular cystic lesion with polypoid mural nodules than endometrioid carcinoma [9–12]. Additionally, CCC exhibits hyperintense cystic components on T1-weighted imaging (T1WI) more frequently than dose high-grade serous carcinomas [13].

The ultrasound findings of CCC have been classified into three subtypes: solid mass, unilocular-solid cyst, and multilocular-solid cyst [6]. To the best of our knowledge, there are no reports describing the MRI features of a completely solid CCC, which typically presents a band-like peripheral area with a central geographic region. This pattern allows for visualization of the renal corticomedullary structure. Here we describe two cases of entirely solid ovarian CCC and present the correlation between MRI features and pathological findings for both cases.

Case 1

A 61-year-old woman presented with atypical genital bleeding and a palpable mass in the lower abdomen that had persisted for 1 month. Laboratory tests revealed no abnormalities in blood or biochemical markers, except for an elevated serum carbohydrate antigen (CA) 125 level. A high serum CA125 level of 759.1 IU/mL (normal value: < 37 IU/mL) was observed. The patient had undergone a right salpingo-oophorectomy for an ovarian cystadenoma 22 years back. Her family history was unremarkable.

A well-circumscribed, oval tumor with a diameter of approximately 24 cm, a band-like peripheral area, and a geographic central area was observed in the left adnexal region on T2-weighted imaging (T2WI) (Fig. 1). Compared to the iliac muscle, the peripheral area of the tumor appeared iso-hyperintense, isointense, hyperintense, and hypo-isointense on T2WI, unenhanced T1WI, diffusion-weighted imaging (DWI), and an apparent diffusion coefficient (ADC) map, respectively, and it showed gradually increasing enhancement on dynamic contrast-enhanced T1WI. The central area of the tumor appeared hyperintense, hypointense, hypointense, hyperintense, and less enhanced on T2WI, T1WI, DWI, an ADC map, and dynamic contrast-enhanced T1WI, respectively. By placing a region of interest measuring 40 mm^2, the ADC value ranged from 1.08 to 1.27 mm^2/second for the peripheral area of the tumor and from 2.55 to 2.73 mm^2/second for the central area.

A simple total hysterectomy, left salpingo-oophorectomy, and partial omentectomy were performed. The cut surface of the resected specimen revealed a solid component throughout the tumor, with a small hemorrhage at the upper pole and a hemorrhagic cyst coexisting with endometriosis at the left pole. No pelvic endometriosis was observed. Hematoxylin and eosin (HE) staining of the peripheral aera of the tumor showed that cancer cells proliferated in a tubulocystic pattern, ranging from large ectatic cysts to small, round, and nonspecific glandular structures, accompanied by an increase in stromal fibrous tissue. A high-power view revealed tumor cells ranging from the highly atypical clear cell type to the hobnail type without clear cytoplasm. In the central area of the tumor, predominant edematous stroma with minimal fibrosis and cancer cell proliferation was observed. Foci-containing cells with small nuclei and minimal atypia were observed in isolation within the tumor, suggesting borderline malignancy.

The final diagnosis was left ovarian CCC (pT1a). The patient received adjuvant chemotherapy with six cycles of paclitaxel and carboplatin, followed by surgery. No residual tumor or distant metastases were observed for 3 months after the treatment.

Case 2

A 58-year-old woman presented with lower abdominal pain and a palpable mass that had persisted for 1 month, accompanied by atypical genital bleeding. Her medical history included appendicitis at the age of 13 years, hypertension, arrhythmia, a thyroid nodule, and uterine endometriosis. Her family history revealed that her father had bladder cancer and her mother. Had Parkinson's disease. Laboratory tests results were unremarkable, except for an elevated serum CA-125 level (82.9 IU/mL; normal value: < 37 IU/mL).

A well-contoured oval tumor with a diameter of approximately 15 × 20 cm, a band-like peripheral area, and a geographic central area was observed in the left adnexal region on T2WI (Fig. 2). Compared to the iliac muscle, the peripheral

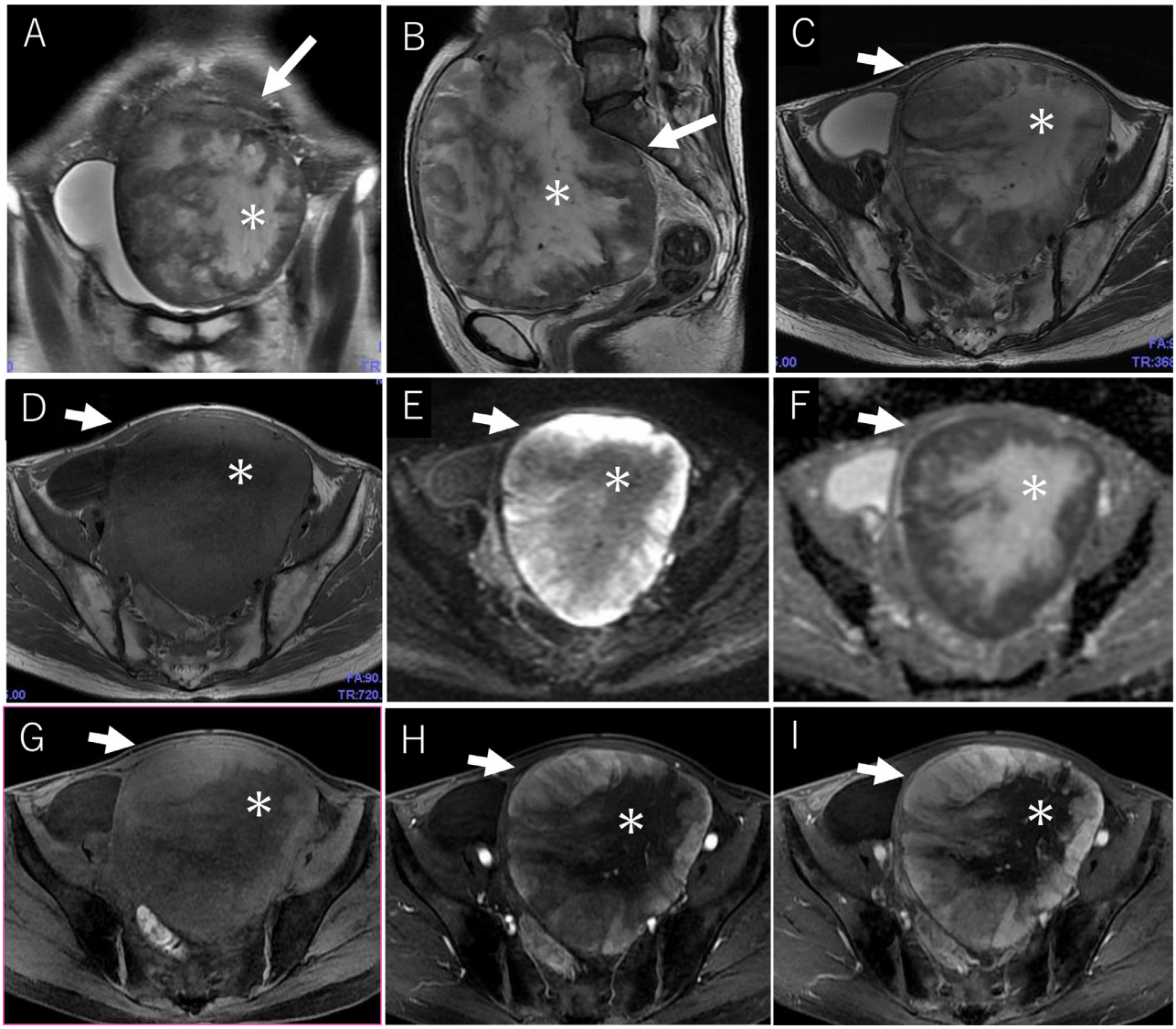

Fig. 1 – Case 1: Clear cell carcinoma of the left ovary in a 61-year-old woman. T2-weighted imaging in the axial (A), sagittal (B), and coronal (C) planes reveal that the tumor comprises a hypointense peripheral area with a band-like structure (arrows) and a hyperintense central area with a geographic structure (asterisks). Compared to the iliac muscle, the peripheral area (arrows) appears isointense on T1-weighted imaging (T1WI) (D), hyperintense on diffusion-weighted imaging (DWI) (E), and hypointense on an apparent diffusion coefficient (ADC) map (F). The central area (asterisks) exhibits hypointensity on both DWI and T1WI and hyperintensity on the ADC map. Multiphasic contrast-enhanced T1WI in the unenhanced (G), early (H), and delayed phases (I) shows gradual enhancement in the peripheral area of the tumor, while the central area demonstrates less enhancement. The ADC value ranges from 1.08 to 1.27 mm^2/sec for the peripheral are and from 2.55 to 2.73 mm^2/sec for the central area. The cut surface of the resected specimen (J) showed an entirely solid component with a small hemorrhage at the upper pole. A hemorrhagic cyst (arrow), coexisting with endometriosis (not shown), is observed within the tumor. The peripheral area shows clusters of large and small cysts on hematoxylin and eosin (HE) staining at low magnification (K); this indicates clear cell carcinoma. At higher magnification (L), cancer cells can be seen proliferating in a tubulocystic pattern, ranging from large ectatic cysts to small, round, and nonspecific glandular structures, accompanied by an increase in stromal fibrous tissue. A high-power view (M) reveals variably confluent small cysts lined by hobnail, flat, and low cuboidal cells without clear cytoplasm. The central area of the tumor (N) shows predominantly edematous stroma with minimal fibrosis and cancer cell proliferation. In areas of glandular proliferation (O), small clusters of cysts containing cells with smaller nuclei and minimal atypia (orange circles) are observed, suggesting borderline malignancy.

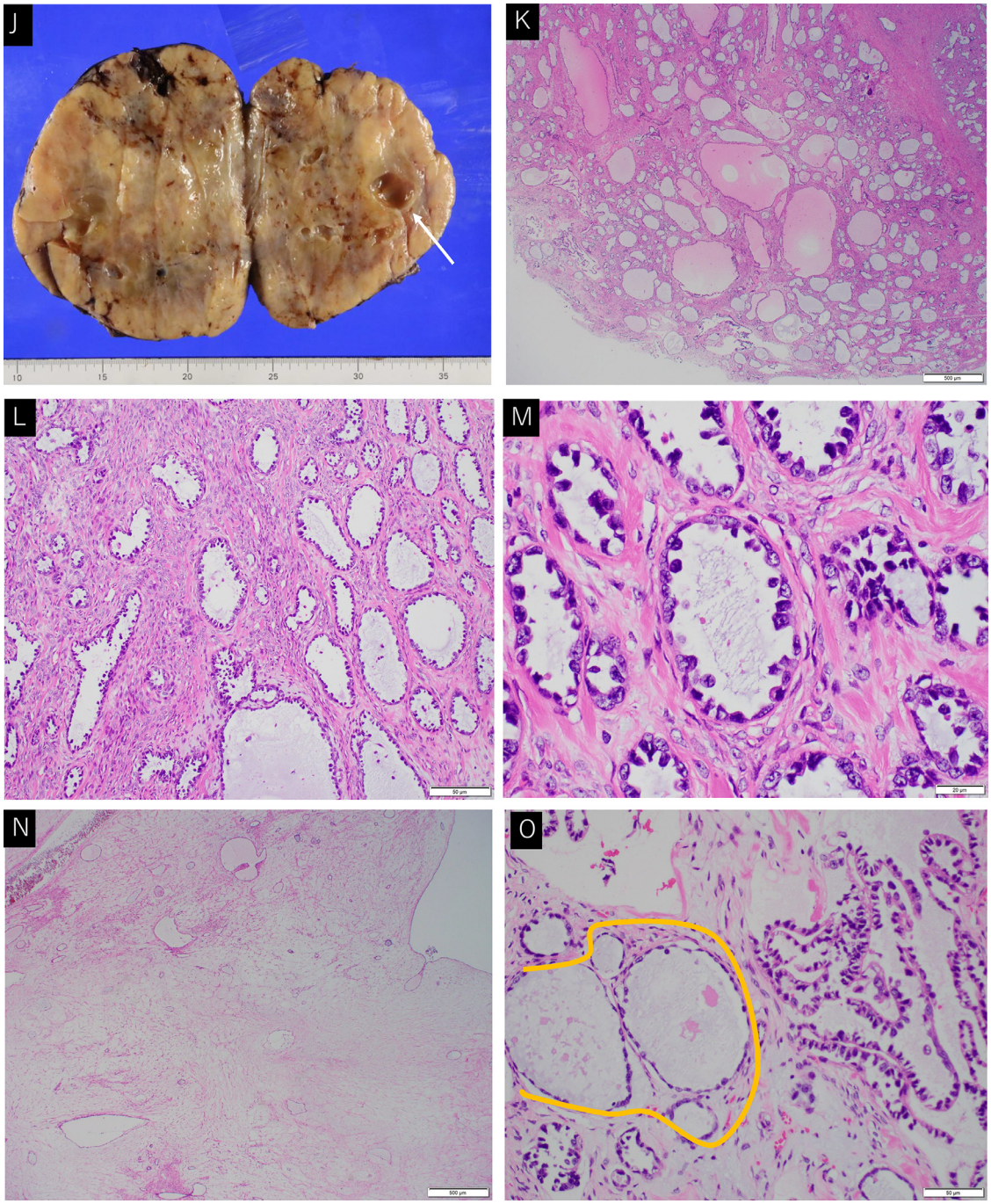

Fig. 1 – Continued

area of the tumor appeared iso-hyperintense, isointense, hyperintense, and hypo-isointense on T2WI, unenhanced T1WI, DWI, and an ADC map, respectively, and it showed gradually increasing enhancement on dynamic contrast-enhanced T1WI. The central area of the tumor appeared hyperintense, hypointense, hypointense, hyperintense, and less enhanced on T2WI, T1WI, DWI, an ADC map, and dynamic contrast-enhanced T1WI, respectively. By placing a region of interest measuring 40 mm^2, the ADC value ranged from 1.39 to 1.68 mm^2/second for the peripheral area of the tumor and 2.36 to 2.64 mm^2/second for the central area.

Simple total hysterectomy, left salpingo-oophorectomy, and partial omentectomy were performed. Macroscopic examination of the resected specimen revealed an entirely solid component with a small hemorrhage at the lower pole. No pelvic endometriosis was observed. In histopathological analysis, HE staining of the peripheral aera showed that the cancer cells proliferated in a solid and nested pattern with

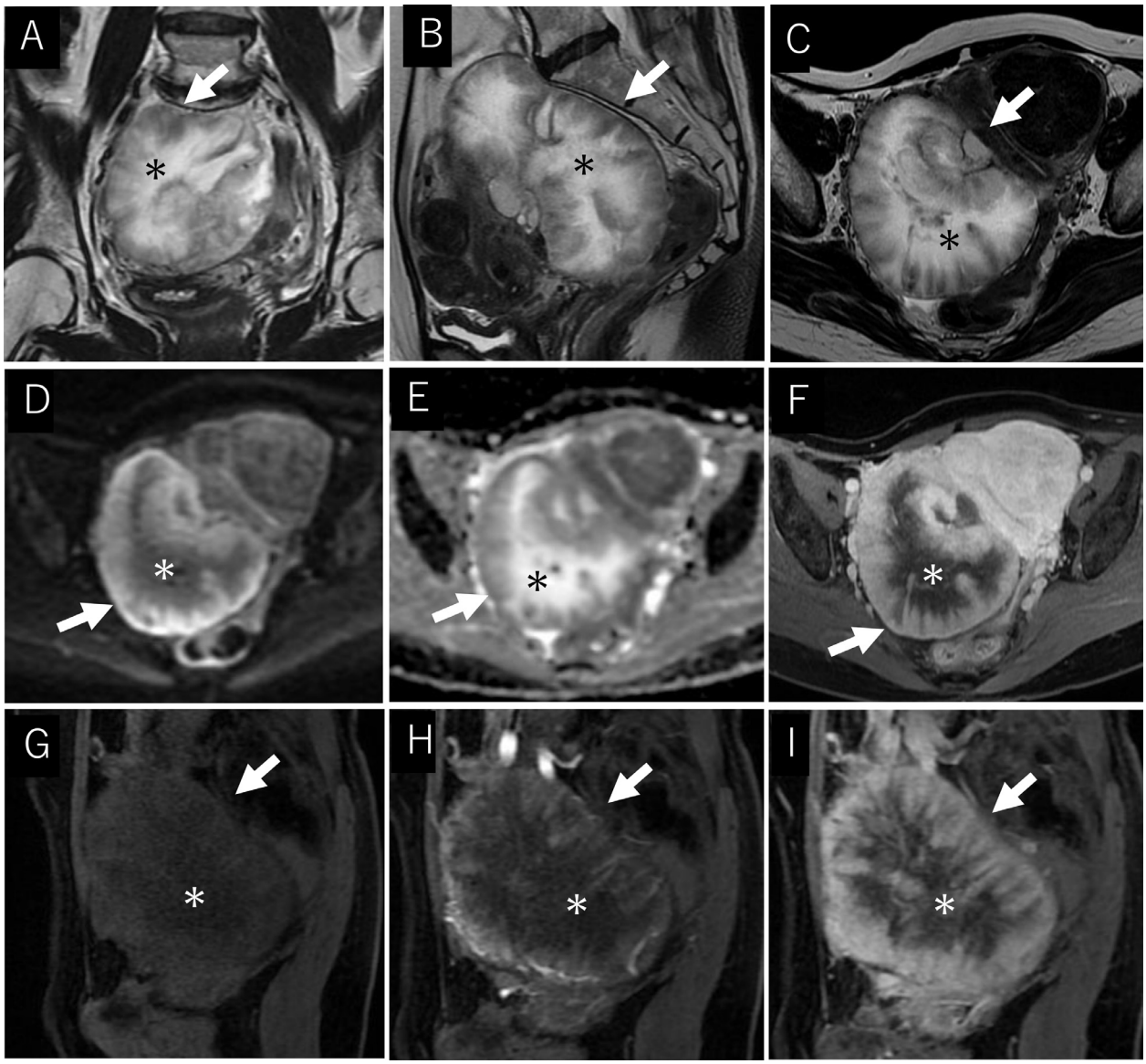

Fig. 2 – Case 2: Clear cell carcinoma of the left ovary in a 58-year-old woman T2-weighted imaging (T2WI) in the axial (A), sagittal (B), and coronal (C) planes show that the tumor is composed of a hypointense peripheral area with a band-like structure (arrows) and a hyperintense central geographic area (asterisks). Compared to myometrium, the peripheral area (arrows) appears hyperintense on diffusion-weighted imaging (DWI) (D), iso-hypointense on an apparent diffusion coefficient (ADC) map (E), and isointense in the contrast-enhanced equilibrium phase (F). The central area (asterisks) shows hypointensity on DWI, hyperintensity on the ADC map, and less enhancement in the contrast-enhanced equilibrium phase. Multiphasic contrast-enhanced T1-weighted imaging (T1WI) in the unenhanced (G), early (H), and delayed phases (I) shows gradual enhancement in the peripheral area of the tumor, whereas the central area exhibits less enhancement. The ADC value ranges from 1.39 to 1.68 mm^2/sec for the peripheral area and from 2.36 to 2.64 mm^2/sec for the central area. The cut surface of the resected specimen (J) reveals an entirely solid component with a small hemorrhage at the lower pole. Hematoxylin and eosin (HE) staining of the peripheral area shows tumor cell proliferation with eosinophilic to clear cytoplasm in a solid, nest-like, or tubular structure at low magnification (K). At a higher magnification (L), tumor proliferation is observed in a solid/nested pattern with interspersed collagenous fibrous tissue resembling septa. The central area displays mesenchymal cell proliferation filling areas of tissue dropout in an edematous background at low magnification (M), and clear cell carcinoma cell proliferation within the edematous stroma with less prominent fibrosis at higher magnification (N).

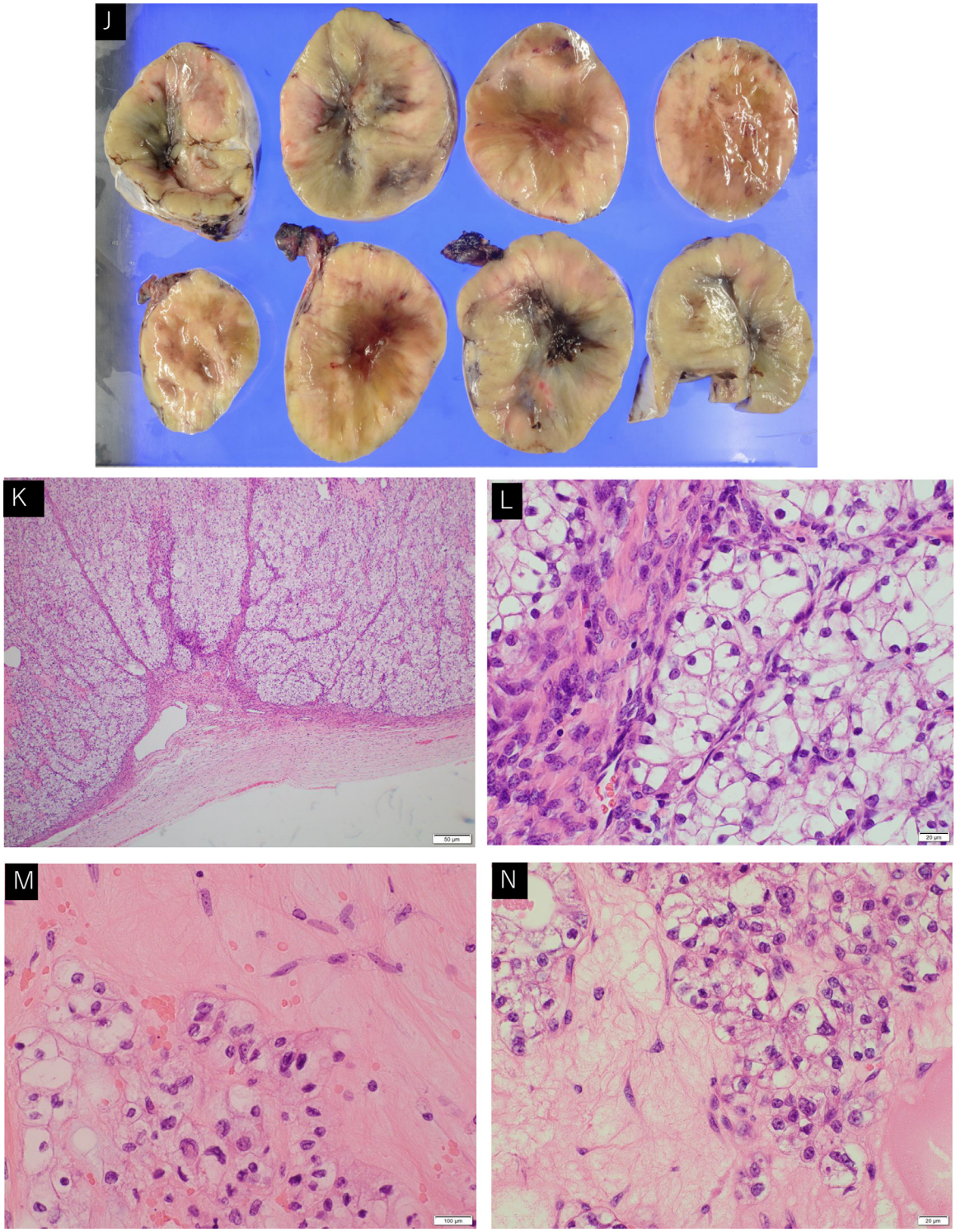

Fig. 2 – Continued

interspersed collagenous fibrous tissue and were surrounded by a fibrous capsule. In the central area of the tumor, predominant edematous stroma was observed with minimal fibrosis and cancer cell proliferation. There was no histopathological evidence of endometriosis. The final diagnosis was right ovarian CCC (pT1a). The patient did not receive adjuvant chemotherapy. No residual tumor or distant metastases was observed for 4.5 years following the surgery.

Discussion

CCC reveals variable MRI findings ranging from solid to cystic characteristics because the MRI features of the solid component vary, reflecting the diversity of tissue structures [5]. When distinguishing CCC from endometrioid carcinoma, two growth patterns of the solid component are often used. Approximately 60%-70% of patients with CCC exhibit the "polypoid, focal, or eccentric" growth pattern, while the remaining 30%-40% may display the "broad-base, multifocal, or concentric" growth pattern [11,14,15]. In the presented cases, MRI findings revealed an entirely solid tumor that did not meet the criteria for "polypoid, focal, or eccentric" or the "broad-base, multifocal, or concentric" growth pattern.

The tumor microstructure is associated with the ADC value (mm^2/second) as a potential imaging marker [16]. The mean (range) ADC value for the peripheral area where the cancer cell proliferation with fibrosis was observed was 1.18 (1.08-1.27) $\times 10^{-3}$ mm^2/second in case 1 and 1.47 (1.39-1.68) $\times$ 10^{-3} mm^2/second in case 2, respectively. These values were consistent with those reported in previous studies using a 1.5 T MRI scanner, which showed values ranging from 0.98 to 1.87 $\times$ 10^{-3} mm^2/second in patients with CCC [17]. The mean (range) ADC value for the central area, where edematous stroma with minimal cancer cell proliferation was observed, was 1.47 (1.39-1.68) $\times 10^{-3}$ mm^2/second in case 1 and 2.64 (2.55-2.73) $\times$ 10^{-3} mm^2/second in case 2; the high value reflects low cellularity with a high volume of extracellular space [15].

Histopathologically, the growth patterns of cancer cells such as nests, tubules, and papillae correlate with the solid component growth pattern on MRI, including "polypoid, focal, or eccentric" patterns. CCCs arising from endometriosis-associated cysts tend to exhibit papillary patterns while those arising from adenofibromas often demonstrate tubulocystic patterns. However, the tubulocystic, papillary, and solid architectures frequently coexist within the tumor [1,2,4]. In case 1, foci containing cells with small nuclei and minimal atypia were observed in isolation within the tumor, suggesting borderline malignancy. However, CCCs often contain a borderline component [1]. Clear cell borderline tumors and adenofibromatous components were not observed in either patient.

CCCs are known to be associated with background ovarian endometriosis in approximately 20%-50% of cases and with more widespread pelvic endometriosis in up to 70% of cases [2]. In this case, neither background ovarian endometriosis nor pelvic endometriosis was observed in either tumor: only hemorrhagic cysts coexisting with endometriosis were present in case 1. In the study by Pozzati et al. [6], both our patients exhibited a solid tumor. Case 1 represented CCC that was associated with endometriosis in the same ovary but had not originated from an endometriotic cyst. Case 2 showed CCC without any clinical or histopathological evidence of endometriosis. Therefore, we believe that the tumor did not originate from endometriotic cysts in both cases. In a study by Kato et al., which included 4 clear cell adenofibroma-associated, 21 endometriosis-associated, and 19 indeterminate CCCs, solid tumors were observed only in the indeterminate CCC groups [18]. Kato et al. defined indeterminate CCCs as a distinct group of tumors that were separate from clear cell adenofibroma- and endometriosis-associated CCCs, and not true subtypes of CCC. The lesions in both our cases could correspond to indeterminate CCCs, as described by Kato et al.

Conclusion

We reported two cases of entirely solid CCC with pT1a stage in woman aged approximately 60 years old; both patients were older than those typically diagnosed with endometriosis-associated CCCs. The origin of tumors in both cases could not be traced to endometriosis or clear cell adenofibroma [6,18]. Moreover, the mechanism underlying the appearance of the peripheral and central areas with renal corticomedullary contrast remains unknown. The findings from this case suggest that MRI can provide valuable insights for the differential diagnosis of epithelial ovarian carcinomas. Further studies are necessary to clarify the pathological structure and origin of CCC.

Patient consent

We have received written informed consent from the two patients to publish this case report and related images.

REFERENCES

[1] Prat J, D'Angelo E, Espinosa I. Ovarian carcinomas: at least five different diseases with distinct histological features and molecular genetics. Hum Pathol 2018;80:11–27. doi:10.1016/j.humpath.2018.06.018.

[2] Fadare O, Parkash V. Pathology of endometrioid and clear cell carcinoma of the ovary. Surg Pathol Clin 2019;12(2):529–64. doi:10.1016/j.path.2019.01.009.

[3] Ushijima K. Current status of gynecologic cancer in Japan. J Gynecol Oncol 2009;20(2):67–71. doi:10.3802/jgo.2009.20.2.67.

[4] Chen JK, Teoh D, Hu JM, Shin JY, Osann K, Kaoo DS. Do clear cell ovarian carcinomas have poorer prognosis compared to other epithelial cell types? A study of 1411 clear cell ovarian cancers. Gynecol Oncol 2008;109(3):370–6. doi:10.1016/j.ygyno.2008.02.006.

[5] Xu L, Lee SI, Kilcoyne A. MR imaging of epithelial ovarian neoplasms part II malignant. Magn Reson Imaging Clin N Am 2023;31(1):53–64. doi:10.1016/j.mric.2022.07.002.

[6] Pozzati F, Moro F, Pasciuto T, Gallo C, Ciccarone F, Franchi D, et al. Imaging in gynecological disease (14): clinical and ultra- sound characteristics of ovarian clear cell carcinoma. Ultrasound Obstet Gynecol 2018;52(6):792–800. doi:10.1002/uog.19171.

[7] Tanaka YO, Okada S, Satoh T, Matsumoto K, Oki A, Saida T, et al. Differentiation of epithelial ovarian cancer subtypes by use of imaging and clinical data: a detailed analysis. Cancer Imaging 2016;16:3. doi:10.1186/s40644-016-0061-9.

[8] Elsherif SB, Bhosale PR, Lall C, Menias CO, Itani M, Butler KA, et al. Current update on malignant epithelial ovarian tumors. Abdom Radiol 2021;46(6):2264–80. doi:10.1007/s00261-021-03081-0.

[9] Tanaka YO, Okada S, Yagi T, et al. MRI of endometriotic cysts in association with ovarian carcinoma. AJR Am J Roentgenol 2010;194(2):355–61. doi:10.2214/AJR.09.2985.

[10] Tanaka YO, Yoshizako T, Nishida M, Yamaguchi M, Sugimura K, Itai Y. Ovarian carcinoma in patients with endometriosis: MR imaging findings. AJR Am J Roentgenol 2000;175(5):1423–30. doi:10.2214/ajr.175.5.1751423.
[11] Morioka S, Kawaguchi R, Yamada Y, Iwai K, Yoshimoto C, Kob- ayashi H. Magnetic resonance imaging findings for discriminating clear cell carcinoma and endometrioid carcinoma of the ovary. J Ovarian Res 2019;12(1):20. doi:10.1186/s13048-019-0497-1.
[12] Ohya A, Fujinaga Y. Magnetic resonance imaging findings of cystic ovarian tumors: major differential diagnoses in five types frequently encountered in daily clinical practice. Jpn J Radiol 2022;40(12):1213–34. doi:10.1007/s11604-022-01321-x.
[13] Ma FH, Qiang JW, Zhang GZ, Li HM, Cai SQ, Rao YM. Magnetic resonance imaging for distinguishing ovarian clear cell carcinoma from high-grade serous carcinoma. J Ovarian Res 2016;9(1):40. doi:10.1186/s13048-016-0251-x.
[14] Taylor EC, Irshaid L, Mathur M. Multimodality imaging approach to ovarian neoplasms with pathologic correlation. RadioGraphics 2021;41(1):289–315. doi:10.1148/rg.2021200086.
[15] Takeyama N, Sasaki Y, Ueda Y, Tashiro Y, Tanaka E, Nagai K, et al. Magnetic resonance imaging-based radiomics analysis of the differential diagnosis of ovarian clear cell carcinoma and endometrioid carcinoma: a retrospective study. Jpn J Radiol 2024;42(7):731–43. doi:10.1007/s11604-024-01545-z.
[16] Winfield JM, Wakefield JC, Doling D, Hall M, Freeman S, JD Bren- ton, et al. Diffusion-weighted MRI in advanced epithelial ovarian cancer: apparent diffusion coefficient as a response marker. Radiology 2019;293(2):374–83. doi:10.1148/radiol.2019190545.
[17] Ono T, Kishimoto K, Tajima S, Maeda I, Takagi M, Suzuki N, et al. Apparent diffusion coefficient (ADC) values of serous, endometrioid, and clear cell carcinoma of the ovary: pathological correlation. Acta Radiol 2020;61(7):992–1000. doi:10.1177/0284185119883392.
[18] Kato H, Hatano Y, Makino H, Furui T, Morishige KI, Matsuo M. Clear cell carcinoma of the ovary: comparison of MR findings of histological subtypes. Abdom Radiol 2016;41:2476–83. doi:10.1007/s00261-016-0777-9.